

# Dynamics of surface directed mesophase formation in block copolymer melts

Sevink, G. J. A.; Zvelindovsky, A. V.; van Vlimmeren, B. A. C.; Maurits, N. M.; Fraaije, J. G. E. M.

*Published in:*
Journal of Chemical Physics

*DOI:*
10.1063/1.477837



*Publication date:*
1999

# Dynamics of surface directed mesophase formation in block copolymer melts

G. J. A. Sevink, A. V. Zvelindovsky, B. A. C. van Vlimmeren, N. M. Maurits, and J. G. E. M. Fraaije

Citation: J. Chem. Phys. **110**, 2250 (1999); doi: 10.1063/1.477837
View online: https://doi.org/10.1063/1.477837
View Table of Contents: http://aip.scitation.org/toc/jcp/110/4
Published by the American Institute of Physics

# Dynamics of surface directed mesophase formation in block copolymer melts

G. J. A. Sevink,[a] A. V. Zvelindovsky,[b] B. A. C. van Vlimmeren, N. M. Maurits, and J. G. E. M. Fraaije
*Faculty of Mathematics and Natural Sciences, University of Groningen, Nijenborgh 4, 9747 AG Groningen, The Netherlands*

(Received 6 August 1998; accepted 23 October 1998)

The dynamic mean-field density functional method is adapted to describe phase separation in the presence of geometrical constraints. We observe that inclusion of small filler particles (such as rods) already has a dramatic effect on the morphology of polymer melts. The effect is comparable to the effect of applied simple steady shear. Mesostructures in the presence of large filler particles such as plates are totally governed by the geometry of the particle. Effects of polymer–surface interactions on morphology formation are investigated in detail. © *1999 American Institute of Physics.* [S0021-9606(99)70704-X]

## I. INTRODUCTION

It is well known that material structures in the mesoscopic domain play an important role in macroscopic material properties. Models that describe the dynamics in the mesoscopic domain are of extreme importance for understanding the relation between processing conditions and particular mesostructures. For instance, a great deal of theoretical and experimental attention has been given to ordering phenomena in block copolymers.[1,2] It was found experimentally that block copolymers are capable of forming mesoscale structures (such as lamellar mesophases) whose morphology can be tailored by controlled synthesis. Mesoscopic models that are used to describe morphology formation at mesoscale level form a bridge between models that describe fast molecular kinetics and slow thermodynamic relaxations of macroscopic properties.

A method for investigating the dynamic formation of mesostructures was recently developed by Fraaije *et al.*[3] It combines a (dynamic) mean-field density functional theory with Gaussian chains as a molecular model. This theory has been validated for specific[4] triblock polymer surfactants: Pluronics L64 $(EO)_{13}(PO)_{30}(EO)_{13}$ and 4R25 $(PO)_{19}(EO)_{33}(PO)_{19}$. Recently, this theory was adapted for describing mesoscale dynamics of block copolymers under shear.[5–7] It is well known that flows affect mesostructures, giving rise to global orientation.[8,9] As a next step in this paper, we consider surface effects due to the presence of solid objects in a block copolymer melt. These surface effects are known to have great influence on the resulting mesostructures. Both shear and surface effects are often present in the experiments. For reasons of simplicity, we only consider surface effects resulting from stationary objects. Moving objects, giving rise to much more complex computer implementations of our parallel algorithms, will be considered in the future.

Many models that are currently used to describe the behavior of polymers are based on traditional free energy expansion methods (Cahn–Hilliard,[10] Oono–Puri,[11] Flory–Huggins–de Gennes[12]). A disadvantage of the use of these models for studies of specific processes is that they contain only the basic physics of phase separation[13] and are not well suited for specific application to different complex industrial and biological liquids. In contrast to these phenomenological theories we do not truncate the free energy expansion, but rather retain the full polymer path integral by a numerical procedure.[13–19] Very recently a similar approach has been also started to use by other authors.[20] The benefit of such an approach is that it allows for the description of the mesoscopic dynamics of *specific* complex polymer liquids.[4]

The morphologies of complex liquids in confined geometries has been the subject of numerous studies both by experimentalists and theoreticians. Several aspects have been considered. Mesostructures in diblock and triblock copolymer thin films are studied because[1,2,21–27] the surface properties of these materials, such as adhesion, friction, and wetting, are controlled by the mesostructures near the surface. For instance, atomic force microscope (AFM) experiments[2] show interesting ordering phenomena in spin-coated films of a commercial triblock copolymer. Cylinders with two kinds of orientation (parallel and perpendicular) are found that are packed in large islands. Related studies have been carried out for mesostructure orientation of block copolymer films when confined between parallel flat plates.[28–30] Hydrodynamic effects on the surface directed phase separation have been studied[31] as well as the effect of patterned surfaces on diblock-copolymer melts.[32] More general studies with respect to several aspects of interaction phenomena of copolymers at surfaces and interfaces are very numerous.[33–42] For example, the dynamics of polymer absorption at a wall has recently been addressed in Ref. 42 using self-consistent field theory. In this article we extend the dynamic density functional method[14,15] to simple surface interactions with stationary filler particles. The advantage of this method with respect to the previously mentioned (phenomenological) methods is that the mesostructure formation in *specific* polymer systems

[a]Electronic mail: sevink@chem.rug.nl
[b]Electronic mail: andrei@chem.rug.nl

 

with *specific* surface interactions can be investigated. Moreover, no simulations of polymer morphology formation with boundary interactions in three dimensions have been performed until this moment. This step is important since in many cases such as the AFM measurements, one wants to relate measurements of the surface morphologies [two-dimensional (2D)] of specific polymers to bulk morphologies (3D). With the help of this extension we can investigate all kinds of interesting phenomena: dependency of the orientation of mesostructures (lamellar, hexagonal, etc) on the surface interactions and confinement of melts between flat plates and filler particles combined with shear. More importantly, the time evolution of the mesophase structures can be followed depending on geometry of filler particles. The filler particles constitute regions where the densities of the different bead types are zero by exclusion. This exclusion effect can be treated by introducing so-called mask fields. In our calculations, the positions of the surface (the positions of the mask field) are bound to the grid elements. For the moment, all simulations are carried out for a symmetric diblock copolymer melt. More specific applications, such as the influence of surface interactions on mesostructures in PL64, will be considered in the future.

## II. METHOD

The polymer melt is modeled as a compressible system, consisting of Gaussian chain molecules in a mean-field environment. The free energy functional for copolymer melts has a form that is similar to the free energy that is used in Refs. 4, 15, and 16:

$$\begin{aligned} F[\{\rho\}] = &-kT\ln\frac{\Phi^n}{n!} - \sum_I \int_V U_I(\mathbf{r})\rho_I(\mathbf{r})d\mathbf{r} \\ &+ \frac{1}{2}\sum_{I,J}\int_{V^2}\epsilon_{IJ}(\mathbf{r}-\mathbf{r}')\rho_I(\mathbf{r})\rho_J(\mathbf{r}')d\mathbf{r}\,d\mathbf{r}' \\ &+ \frac{1}{2}\sum_{I}\int_{V^2}\epsilon_{IM}(\mathbf{r}-\mathbf{r}')\rho_I(\mathbf{r})\rho_M(\mathbf{r}')d\mathbf{r}\,d\mathbf{r}' \\ &+ \frac{\kappa_H}{2}\int_V\left(\sum_I \nu_I[\rho_I(\mathbf{r})-\rho_I^0]\right)^2 d\mathbf{r}, \end{aligned} \tag{1}$$

except for an extra fourth term that contributes only in the direct vicinity of the filler particles. This accounts for the interaction of a polymer melt with surfaces. In this equation, $n$ is the number of polymer molecules, $\Phi$ is the intramolecular partition function for ideal Gaussian chains in an external field $U$, $I$ is a component index, $\rho_I$ are the density fields of the different bead types $I$, and $V$ is the system volume. Inside the filler particles, the densities $\rho_I$ of the different bead types are equal to zero. Since the density $\rho$ is present in all integrals in the definition of the free energy [Eq. (1)], integrals (except ''surface'' term) over the entire volume $V$ are equal to the integrals restricted to $V/V^0$, standing for the total volume $V$ with the exception of the volume taken by the filler particles, denoted as $V^0$. The filler particles considered here are constrained to the condition of stationary position in time. The constant density field $\rho_M$ (where $M$ represents beads of the filler particle type) that appears in Eq. (1) is defined as $\rho_M(\mathbf{r})=1$ for $\mathbf{r}\in V^0$ and $\rho_M(\mathbf{r})=0$ for $\mathbf{r}\in V/V^0$. The average concentration is $\rho_I^0$ and $\nu_I$ is the particle volume. The cohesive interactions have kernels $\epsilon_{IJ}$ $\{\epsilon_{IJ}(|\mathbf{r}-\mathbf{r}'|)=\epsilon_{IJ}^0(3/2\pi a^2)^{3/2}\exp[-(3/(2a^2))(\mathbf{r}-\mathbf{r}')^2]\}$. The surface interactions have kernels $\epsilon_{IM}$. The Helfand compressibility parameter is $\kappa_H$.[16]

The external potentials $U_I$ are conjugate to the densities $\rho_I$ via the Gaussian chain density functional.[15] For our system, Eq. (1), the statistical distribution function of a chain of $N$ beads, in a certain conformation specified by the coordinates of the beads $\{\mathbf{R}_1,\cdots,\mathbf{R}_N\}$ is[3]

$$\begin{aligned} \Psi(\mathbf{R}_1,\cdots,\mathbf{R}_N) = \frac{1}{\Phi}\exp-\Bigg(&\frac{3}{2a^2}\sum_{s=2}^{N}(\mathbf{R}_s-\mathbf{R}_{s-1})^2 \\ &+\sum_{s'=1}^{N}U_{s'}(\mathbf{R}_{s'})\Bigg), \end{aligned} \tag{2}$$

where the external fields $U_{s'}$ are in units $kT$ and $a$ is the Gaussian bond strength parameter. The ensemble average particle density $\rho_s(\mathbf{r})$ of a certain bead $s$ at position $\mathbf{r}$ in space is

$$\begin{aligned} \rho_s[U](\mathbf{r}) = C\mathcal{M}(\mathbf{r})\int_{V^N}&\Psi(\mathbf{R}_1,\cdots,\mathbf{R}_N) \\ &\times\delta(\mathbf{r}-\mathbf{R}_s)d\mathbf{R}_1\ldots d\mathbf{R}_N, \end{aligned} \tag{3}$$

where $C$ is a normalization constant (see Ref. 3) and a mask field $\mathcal{M}(\mathbf{r})$ is used that is defined as

$$\mathcal{M}(\mathbf{r}) = \begin{cases} 0 & \mathbf{r}\in V^0 \\ 1 & \mathbf{r}\in V/V^0. \end{cases}$$

The density functional can be calculated via Green propagators (see Ref. 19 for details)

$$\rho_s(\mathbf{r}) \propto G_s(\mathbf{r})\sigma[G_{s+1}^{\mathrm{inv}}](\mathbf{r}). \tag{4}$$

The set of once integrated Greens functions $G_s(r)$ and $G_{s+1}^{\mathrm{inv}}(r)$ are related by the recurrence relations

$$\begin{aligned} G_s(\mathbf{r}) &= \mathcal{M}(\mathbf{r})e^{-U_s(\mathbf{r})}\sigma[G_{s-1}](\mathbf{r}), \\ G_s^{\mathrm{inv}}(\mathbf{r}) &= \mathcal{M}(\mathbf{r})e^{-U_s(\mathbf{r})}\sigma[G_{s+1}^{\mathrm{inv}}](\mathbf{r}), \end{aligned} \tag{5}$$

where $G_0(\mathbf{r})=G_{N+1}^{\mathrm{inv}}(\mathbf{r})=1$. The linkage operator $\sigma=\sigma[f](\mathbf{r})$ is defined as a convolution with a Gaussian kernel

$$\sigma[f](\mathbf{r}) = \left(\frac{3}{2\pi a^2}\right)^{2/3}\int_V e^{-(3/(2a^2))(\mathbf{r}-\mathbf{r}')^2}f(\mathbf{r}')d\mathbf{r}'. \tag{6}$$

The time evolution of the density field $\rho_I(\mathbf{r})$ can be described by a time dependent Landau–Ginzburg type equation[8,43]

$$\frac{\partial\rho_I}{\partial t} = M_I\nabla\cdot\rho_I\nabla\mu_I + \eta_I. \tag{7}$$

Here $\mu_I=\delta F/\delta\rho_I$ is the intrinsic chemical potential, $M_I$ is a mobility, and $\eta_I$ is a stochastic noise which is distributed according to the fluctuation–dissipation theorem.[18]

The boundary conditions that are used on the simulation box are periodic boundary conditions. For the diffusion flux

in the vicinity of the filler particles, rigid-wall boundary conditions are used. A simple way to implement these boundary conditions in accordance with the conservation law is to allow no flux through the filler particle surfaces, i.e.,

$$\nabla \mu_I \cdot \mathbf{n} = 0, \tag{8}$$

where $\mathbf{n}$ is the normal pointing towards the filler particle. It is easy to show that with these boundary conditions on the filler particles, the free energy decreases with time (neglecting the contribution of the noise):

$$\begin{aligned}\frac{\partial F}{\partial t} &= \int_{V/V^0} \sum_I \frac{\delta F}{\delta \rho_I} \frac{\partial \rho_I}{\partial t} dV \\ &= \int_{V/V^0} \sum_I \mu_I \frac{\partial \rho_I}{\partial t} dV = \int_{V/V^0} \sum_I \mu_I M_I \nabla \rho_I \nabla \mu_I dV \\ &= \sum_I M_I \int_{\partial(V/V^0)} \mu_I \rho_I \nabla \mu_I \mathbf{n}\, dS \\ &\quad - \sum_I M_I \int_{V/V^0} \rho_I (\nabla \mu_I)^2 dV \leqslant 0,\end{aligned} \tag{9}$$

where we have used Gauss' theorem. Since we use a 27 point stencil for the calculation of derivatives, the presence of filler particles affects only the grid elements one cell away from the rigid boundaries.[19]

The same boundary conditions apply to the noise $\eta_I$. The noise has a Gaussian distribution with moments dictated by the fluctuation–dissipation theorem, and is equal to[18] (in the notation of that paper)

$$\eta_I(\mathbf{r},t) = \sqrt{\frac{2}{\beta}} \nabla_r \cdot \sqrt{M_I \rho(\mathbf{r})}\, w_K(\mathbf{r},t), \tag{10}$$

where $w_K$ is a completely decorrelated random field with Gaussian distribution

$$\begin{aligned}&\langle w_I^c(r,t) \rangle = 0, \\ &\langle w_I^c(r,t) w_J^{c'}(r',t') \rangle = \delta_{IJ} \delta_{cc'} \delta(r-r') \delta(t-t').\end{aligned} \tag{11}$$

For the numerical integration of Eq. (7) a Crank–Nicolson scheme is used. Starting configurations for the time integration are homogeneous density distributions and the external field is equal to zero.

## III. RESULTS AND DISCUSSION

As an example, we simulate the behavior of a model polymer which is represented by an $A_8B_8$ Gaussian chain. For all simulations, a cubic grid of dimension $L \times L$ (2D) or $L \times L \times L$ (3D) is used. The dimensionless parameters that are used in the numerics are chosen to be similar to the ones used in Ref. 5. They are:[15,4] the mesh size $h$ of the physical grid equal to $h = 0.7$ nm, the dimensionless time step $\Delta\tau = \beta^{-1} M h^{-2} \Delta t = 0.2$ ($\Delta t = 10$ ns), and a bond length $a$ given by the optimal value[19] of the grid parameter $d = a h^{-1} = 1.1543$. The noise scaling parameter $\Omega = \nu^{-1} h^3 = 100$, with $\nu$ the bead volume which in our case is taken equal for all bead species (see also Refs. 3 and 4 for more details). The exchange parameter is chosen to be equal to $\beta \epsilon_{AB} \nu^{-1} = 1.0$ ($\epsilon_{AA} = \epsilon_{BB} = 0$) and the compressibility parameter $\kappa' = \beta \kappa_H \nu = 12.0$. The diffusion coefficient $D$ that is related to the mobility $M$ by $D_I = \beta^{-1} M_I$ is chosen equal to $D_I = 10^{-11}\,\mathrm{m}^2/\mathrm{s}$ for both bead species. The surface related interaction parameters $\beta \epsilon_{AM} \nu^{-1}$ and $\beta \epsilon_{BM} \nu^{-1}$ are chosen to be different in the different simulations. Taking into account noise and compressibility is important for creating a physically realistic model. We have discussed their effect on phase separation in detail earlier.[16,18]

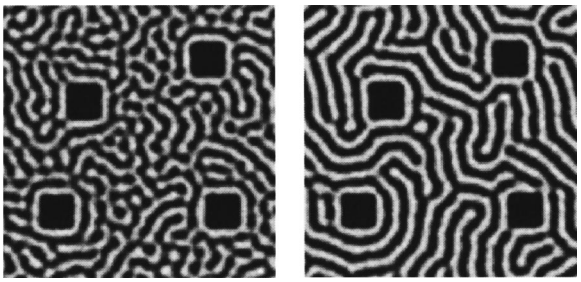

FIG. 1. Two dimensional simulation of $A_8B_8$ block copolymer melt in $128 \times 128$ box in the presence of four filler particles: (a) left: early stage at $\tau = 250$, (b) right: final stage at $\tau = 2000$.

First we consider a simulation in two dimensions ($L = 128$) (Fig. 1). The filler part of the melt consist of four block-shaped particles of $12 \times 12$ grid cells each. The subsequent interaction parameters are chosen equal to $\beta \epsilon_{AM} \nu^{-1} = 4.0$ and $\beta \epsilon_{BM} \nu^{-1} = 0.0$. Note that in the incompressible case the surface contribution in the free energy, Eq. (1), reduces to a constant, if these two parameters are equal.

In Fig. 1(a) the results are shown at an early stage ($\tau = 250$). One clearly observes the phase separation that starts to take place. Around the filler particles surface directed microphase separation can be seen. Closed lamellae parallel to the filler particles surface start to form. At a later stage the lamellae become more distinct and grow in length until most of them span the whole box. In Fig. 1(b) we show the final stage at $\tau = 2000$. It can be observed that the orientation of the lamellae is determined to a great extent by the orientation of the filler particles.

After having observed the process of formation and orientation of lamellae in two dimensions, we now look at a 3D case. In all three-dimensional examples considered, the box parameter $L = 32$. First we consider two cases (displayed in Figs. 2 and 4) where the filler particles are almost identical. In Fig. 2(a), the field $\mathcal{M}(\mathbf{r})$ is shown for a filler particle consisting of a plane ($30 \times 30 \times 1$ grid cells) in the Cartesian $x$ and $y$ directions. The interaction parameters are chosen to be equal to $\beta \epsilon_{AM} \nu^{-1} = -1.0$ and $\beta \epsilon_{BM} \nu^{-1} = 1.0$. These parameters will be used in all the following simulations (where interaction between filler particle and polymer melt is present). This plane almost spans the box, leaving slots at either sides of the plane of one grid cell wide. A $z$ projection of a part of the total three-dimensional space is shown in Fig. 2(b). The slots between the planes can clearly be observed. In this case, the pattern periodicity of the surface is 30. In contrast, in Fig. 4(a), the mask field is shown for a filler particle consisting of a plane ($32 \times 32 \times 1$) that spans the whole box.

As can be seen from Figs. 2(c) ($\tau = 500$) and 2(d) ($\tau$

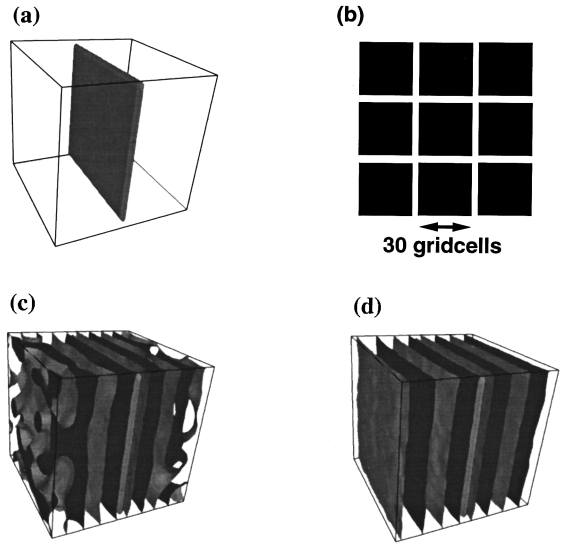


FIG. 2. Lamellar formation of an $A_8B_8$ copolymer melt in the presence of square plates of one grid cell thickness. The interaction of polymer blocks with the surface is $\beta\epsilon_{AM}\nu^{-1}=-1.0$ and $\beta\epsilon_{BM}\nu^{-1}=1.0$: (a) view of filler particle in simulation box, (b) space filled with filler particles (the slots between filler particles are drawn as white lines), (c) morphology of *A* beads (isolevel $\nu\rho_A=0.5$) in one simulation box at $\tau=500$, (d) same for $\tau=2000$.

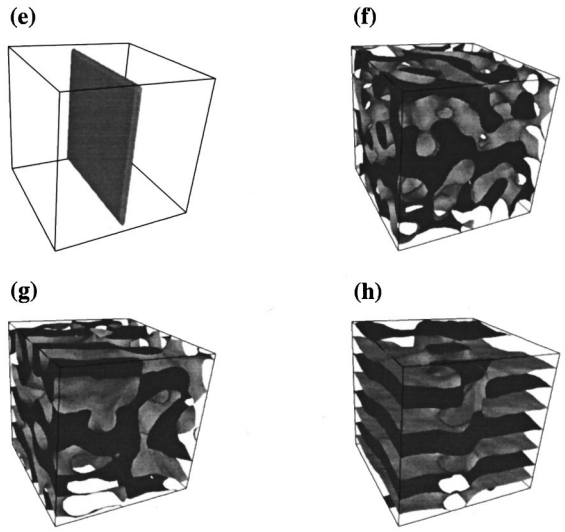


FIG. 3. Lamellar formation of an $A_8B_8$ copolymer melt in the presence of the same filler particle as the previous figure. Moreover, there is no interaction between the polymer beads and boundaries of the filler particles: (e) view of filler particle in simulation box, (f) morphology of *A* beads (isolevel $\nu\rho_A=0.5$) in one simulation box at $\tau=500$, (g) same for $\tau=4000$, (h) final morphology at $\tau=10\,000$.

$=2000$), the presence of the filler particle results in lamellae parallel to the filler particles surface. Parallel lamellae start to form close to the filler particle and spread through the melt. When closely examined, the slots result is a slight bending of the lamellae at the edges of the lamellae [Fig. 2(d)]. One should note that the time scales on which the lamellae are formed are much shorter than the time scales of lamellae formation in the absence of this filler particle.[5] Thus, the presence of surfaces speeds up the formation of mesophase formation enormously.

In the absence of surface interactions, we may observe the influence of confinement (by the filler particle) on the resulting mesostructures of the polymer material. At the same time, we get a feeling of the influence of surface interactions on the orientation of the final morphologies. For this purpose, we consider the same filler particle as before, the mask field of which is shown in Fig. 2(a), and take $\epsilon_{AM}=\epsilon_{BM}=0.0$. Given the mask field of Fig. 3(e) [the same as in Fig. 2(a) but different observation angle] we see in Fig. 3(f) that at $\tau=500$ a structure appears without apparent global orientation. If we compare this with the structure shown in Fig. 2(c) at the same stage, we conclude that surface interaction is, especially in the early stages of phase separation, apparently responsible for speeding up the mesophase formation. At $\tau=4000$ [Fig. 3(g)], where the previous example with boundary interaction already reached the stage of perfect (slightly bended) lamellae parallel to the boundary surface, we see larger structures but still no general global orientation. Only at $\tau=10\,000$ [Fig. 3(h)] do we observe a global orientation *perpendicular* to the surface of the filler particle. Although such orientation requires more investigation, we note that the system is confined between two plates (due to the box periodicity) that act as a strong regularization of the lammelar spacing and orientation. For the hexagonal cylindrical phase perpendicular orientation has been observed in experiments with thin polymer films.[2] We conclude that introducing surface interactions induces fast mesostructure formation, with an orientation mainly directed by the interaction parameters.

In the case of a melt between two planes that are infinite in two Cartesian dimensions (Fig. 4) and the same $\epsilon_{AM}$ and $\epsilon_{BM}$ as before in Fig. 2, we observe fast convergence to a stable morphology. Lamellae start to form immediately after the quench [Fig. 4(b) for $\tau=250$], their number increasing with time and stable in time. At $\tau=1000$ [Fig. 4(c)] we ob-

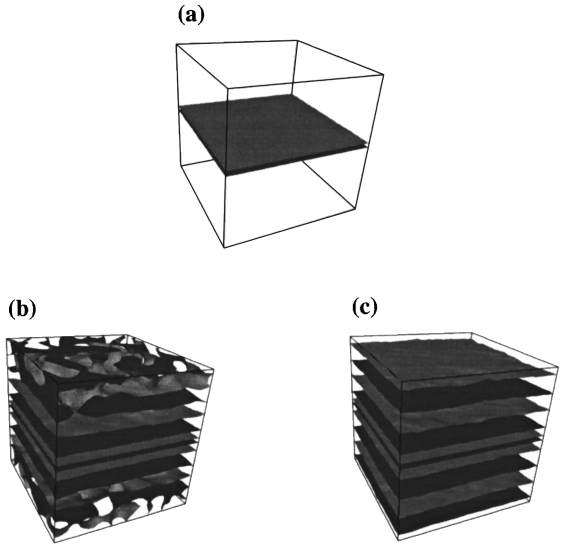


FIG. 4. Lamellar formation of an $A_8B_8$ copolymer melt in the presence of infinite planes of one grid cell thickness: (a) view of the filler particle in the simulation box, (b) morphology of *A* beads (isolevel $\nu\rho_A=0.5$) at $\tau=250$, (c) same for $\tau=1000$.

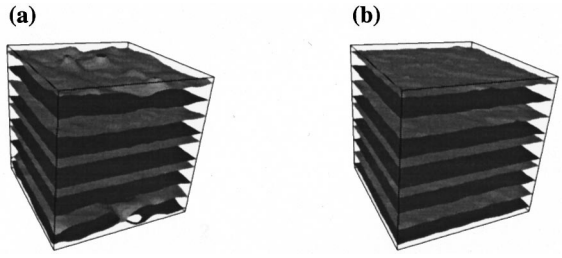


FIG. 5. Same as in Fig. 4 but for thicker infinite planes (four grid cells thick): (a) morphology of $A$ beads (isolevel $\nu\rho_A=0.5$) at $\tau=250$, (b) same for $\tau=1500$.

serve five lamellae of slightly different thickness, especially two very thin ones at the filler particle boundaries. When we consider only a different thickness of the filler particle (a plane of $32\times32\times4$ grid cells), we observe the same number of lamellae at the same time [Fig. 5(a) at $\tau=250$ and Fig. 5(b) at $\tau=1500$] because the width of the lamellae has decreased.

In order to take a closer look at the influence of roughness, we now consider a filler particle that simulates a ''rough'' plate, shown in Fig. 6(a). The mask field $\mathcal{M}(\mathbf{r})$ consists of a plane $(32\times32\times1)$ spanning the whole box,

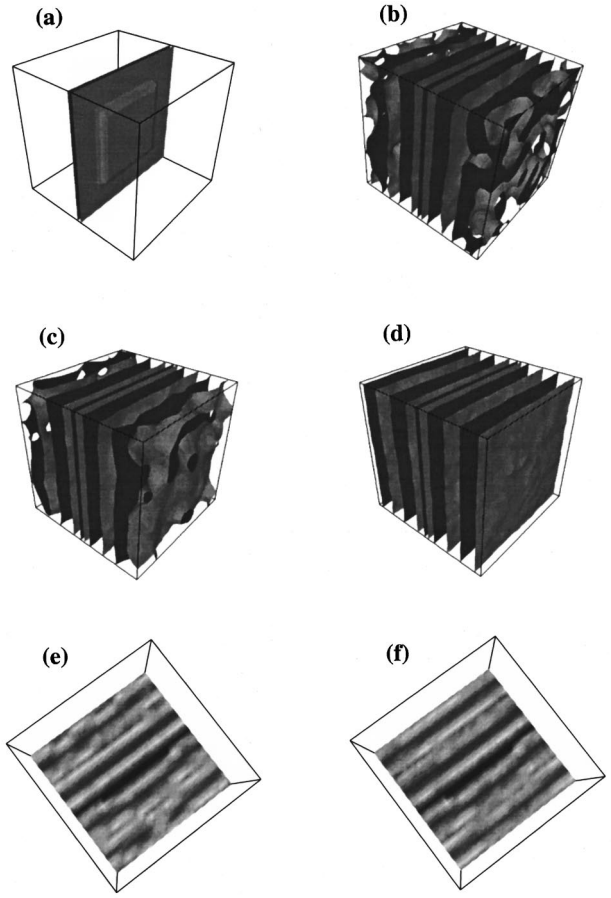


FIG. 6. Lamellar formation of $A_8B_8$ copolymer melt in the presence of a ''rough'' plane: (a) view of the filler particle in the simulation box, (b) morphology of $A$ beads (isolevel $\nu\rho_A=0.5$) at $\tau=250$, (c) same for $\tau=500$, (d) final stage at $\tau=2500$, (e) orthoslice through the middle of the box of the morphology shown in (c), (f) orthoslice for (d).

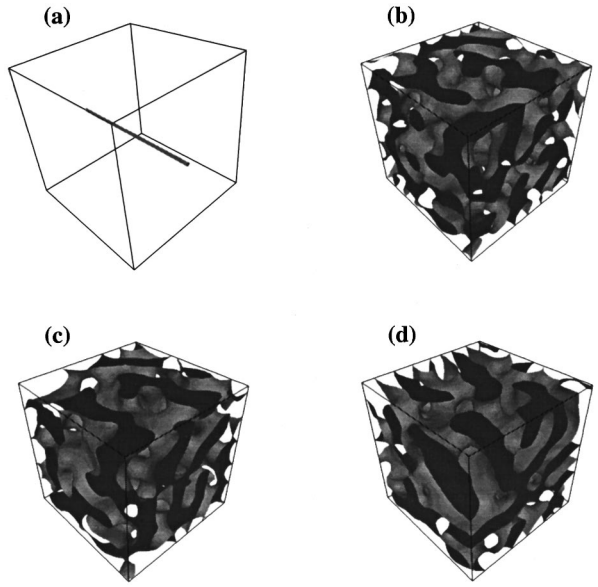


FIG. 7. Mesoscale formation of $A_8B_8$ copolymer melt in the presence of one infinite rod. The interaction of polymer blocks with the surface is $\beta\epsilon_{AM}\nu^{-1}=-1.0$ and $\beta\epsilon_{BM}\nu^{-1}=1.0$: (a) view of the filler particle in the simulation box, (b) morphology of $A$ beads (isolevel $\nu\rho_A=0.5$) at $\tau=500$, (c) same for $\tau=2000$, (d) final stage at $\tau=4000$.

with a smaller plane $(18\times18\times1)$ on top. From a comparison of the result at $\tau=250$ [Fig. 6(b)] of this simulation and the result at $\tau=250$ of a ''smooth'' filler particle [Fig. 4(b)] we see that the influence of the roughness in the early stages is not clearly visible. In Fig. 6(c), the result is shown at $\tau=500$. The morphology is clearly different from the morphologies in Fig. 4: the formation of parallel lamellae takes place at a much smaller rate as in the ''smooth'' case. At $\tau=2500$ [Fig. 6(d)], one can clearly observe a final state of almost parallel lamellae. The process of parallelization can even be considered more closely in Figs. 6(e) and 6(f), where orthogonal slices halfway through the box of the same morphologies [$\tau=500$ in Fig. 6(e) and $\tau=2500$, Fig. 6(f)] can be seen.

Another type of filler particle that has been considered is a rod. In Fig. 7(a) the mask field $\mathcal{M}(\mathbf{r})$ is shown for one infinite rod. At $\tau=500$ [Fig. 7(b)] large structures without apparent global orientation are present. At later times $\tau=2000$ [Fig. 7(c)] and $\tau=4000$ [Fig. 7(d)] larger structures are formed with an orientation that is apparently parallel to the rod. However, close examination of the resulting structures (not shown here) shows clusters of different orientations (parallel, perpendicular).

The configuration of Fig. 7(d) can be used as a starting configuration for the application of simple steady shear.[5] Although the theory considered here is only applicable to stationary objects, we can apply shear in the direction of the rod due to the infinite length of the rod in the direction of the flow. The dimensionless shear rate is chosen equal to $\tilde{\gamma}=0.001$ (for details see Ref. 5). In Fig. 8(a), the configuration is shown at $\tau=5000$. A global orientation starts to develop. This orientation becomes more apparent at later times [Fig. 8(b) at $\tau=7500$ and Fig. 8(c) at $\tau=10\,000$]. The final global orientation is one of almost parallel lamellae that are

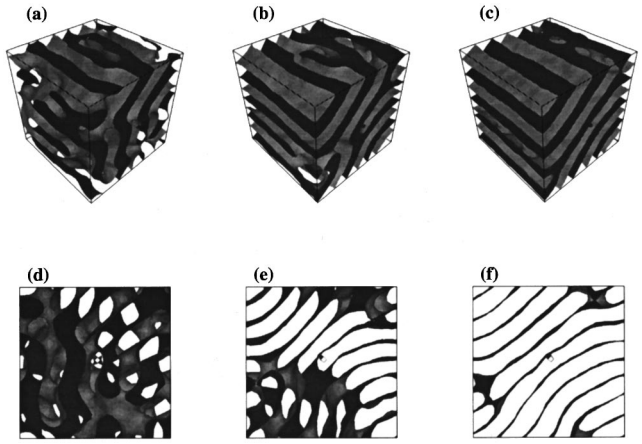


FIG. 8. Lamellar formation of the melt of Fig. 7 in the presence of shear in the direction of the rod. The conformation of Fig. 7(d) is taken as a starting structure: (a) morphology of $A$ beads (isolevel $\nu\rho_A=0.5$) at $\tau=5000$, (b) Same for $\tau=7500$, (c) final stage at $\tau=10\,000$, (d) projection in the direction of shear of the morphology shown in (a), (e) projection of (b), (f), projection of (c).

under a 45° angle with the shearing direction. From the orthogonal projections in Figs. 8(d), 8(e) and 8(f), it can be seen that the lamellae are slightly bent. However, we have found from previous experiments that the global orientation is in this case much affected by the rather small box size ($L=32$). Tilted lamellae are known to be governed by the size of the box. Given the influence of one rod (the volume fraction of rods $V^0/V$ is about 0.1%) we will now consider the influence of a few (in our case, six) randomly positioned rods (the volume fraction is about 0.6%). In Fig. 9(a), the position of the rods can be observed. Again, shear is applied at $\tau=4000$ in the direction of the rods. The same shear rate is used as in the previous example. From Figs. 9(b) and 9(d), where the morphology and the orthogonal projection in the direction of the rods is shown for $\tau=4000$, we conclude that parallel lamellae are formed with a clear global orientation. This orientation is to a large extent governed by the presence

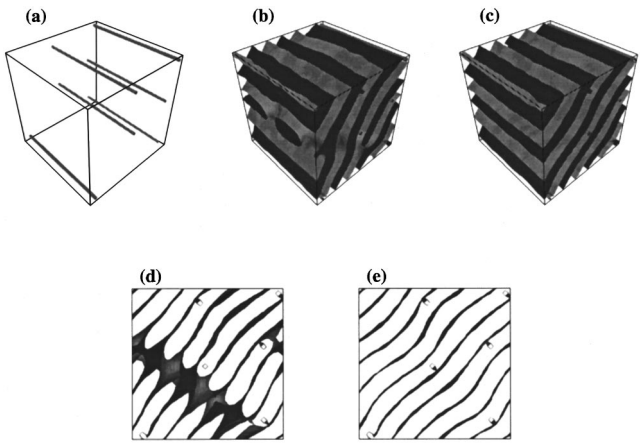


FIG. 9. Lamellae formation of $A_8B_8$ copolymer melt in the presence of six infinite rods: (a) view of the filler particles in the simulation box, (b) morphology of $A$ beads (isolevel $\nu\rho_A=0.5$) at $\tau=4000$ [comparable in time to Fig. 7(d)]. At $\tau=4000$, shear is applied with the same shear rate as in Fig. 8, (c) final structure for $\tau=5750$, (d) projection in the direction of shear of the morphology shown in (b), (e) projection of (c).

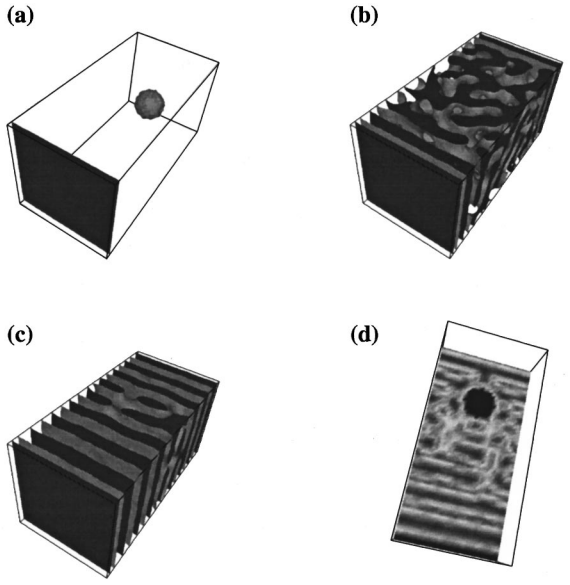


FIG. 10. Lamellae formation of $A_8B_8$ copolymer melt in the presence of a plane and a spherical particle. The interaction of polymer blocks with the surface is $\beta\epsilon_{AM}\nu^{-1}=-1.0$ and $\beta\epsilon_{BM}\nu^{-1}=1.0$: (a) view of the filler particles in the simulation box, (b) morphology of $A$ beads (isolevel $\nu\rho_A=0.5$) at $\tau=250$, (c) final stage at $\tau=2500$, (d) orthoslice through the middle of the box of the morphology shown in (c).

of the rods, since the rods can be observed to be in the middle of $A$ rich regions, and therefore can be considered responsible for the particular bending of the lamellae. The ordering is similar to the ordering in Fig. 8(e), so that we conclude that the process is *twice* as fast, not even taking *shear* into account. At the final stage at $\tau=5750$ [shown in Figs. 9(c) and 9(e)] almost perfect lamellae are formed. Defects are removed by the shear, but the local bending of the lamellae is not affected, and it can be concluded to be caused by the presence of the rods.

As a final example, we consider the effect of a plane ($2\times32\times32$ grid cells) combined with an almost spherical particle (with a radius of five grid cells). The box-size is chosen to be noncubic: $64\times32\times32$. In Fig. 10(a), the mask field $\mathcal{M}(\mathbf{r})$ is shown. At $\tau=250$ [Fig. 10(b)] lamellae parallel to the plane start to form. At $\tau=2500$ [Fig. 10(c)] we observe that these lamellae span the whole box, apart from a very tiny region where the spherical particle is present. From an orthogonal slice at $\tau=2500$ [shown in Fig. 10(d)] we conclude that the parallel orientation is due to the presence of the plate. This orientation is too strong to be affected by the presence of the spherical particle.

## IV. CONCLUDING REMARKS

Here we have extended the dynamic density functional method formulated before for unconfined block copolymer melts[3] to the same systems in the presence of different surfaces. The free energy functional includes an extra term which describes interactions of polymer beads with a surface. In the present paper we focus on the surface directed phase separation itself and limit ourselves to the case of immobile surfaces. With this limitation, we are still able to investigate a large number of interesting phenomena. The

analysis of moving colloidal particles in the polymer environment, implying moving boundary conditions, is left to future publications. Time evolution of mesoscopic block copolymer morphologies is studied using time dependent Landau–Ginzburg type equations for the densities of polymer blocks. Noise and compressibility of the system are explicitly taken into account. Simulations of different systems are performed in 2D and 3D. They include random positioned square-like filler particles in 2D, infinite and finite plane boundaries in 3D, rough surfaces, cylindrical rods, and combined geometries like a sphere near a wall. A simple case of a system under shear is considered as well. We observe a large influence of small filler particles such as infinite rods. These filler particle limit the degrees of freedom in which mesostructures can orient themselves, and therefore lead to perfect lamellae already at a very early stage. Shear and filler particles have similar influences on the conformational behavior, as can be seen from a copolymer melt with one and six rods. More generally, inserting a surface into a diblock copolymer melt induces order in the system and speeds up mesophase separation enormously. The analysis of other polymer systems in the presence of surfaces is in progress.

## ACKNOWLEDGMENTS

Two of the authors (G.J.A.S. and A.V.Z.) acknowledge the support of the MesoDyn project ESPRIT No. EP22685 of the European Community. Discussions with Henk Huinink are gratefully appreciated.

[1] R. van den Berg, H. de Groot, M. A. van Dijk, and D. R. Denley, Polymer **35**, 5778 (1994).
[2] M. A. van Dijk and R. van den Berg, Macromolecules **28**, 6773 (1995).
[3] J. G. E. M. Fraaije, B. A. C. van Vlimmeren, N. M. Maurits, M. Postma, O. A. Evers, C. Hoffmann, P. Altevogt, and G. Goldbeck-Wood, J. Chem. Phys. **106**, 4260 (1996).
[4] B. A. C. van Vlimmeren, N. M. Maurits, A. V. Zvelindovsky, G. J. A. Sevink, and J. G. E. M. Fraaije, Macromolecules (accepted for publication).
[5] A. V. Zvelindovsky, G. J. A. Sevink, B. A. C. van Vlimmeren, N. M. Maurits, and J. G. E. M. Fraaije, Phys. Rev. E **57**, R4879 (1998).
[6] A. V. Zvelindovsky, G. J. A. Sevink, B. A. C. van Vlimmeren, N. M. Maurits, and J. G. E. M. Fraaije, Prog. Colloid Polym. Sci. **110**, 251 (1998).
[7] A. V. Zvelindovsky, G. J. A. Sevink, B. A. C. van Vlimmeren, N. M. Maurits, and J. G. E. M. Fraaije, J. Chem. Phys. **109**, 8751 (1998).
[8] H. Kodama and M. Doi, Macromolecules **29**, 2652 (1996).
[9] G. H. Fredrickson, J. Rheol. **38**, 1045 (1994).
[10] J. W. Cahn and J. E. Hilliard, J. Chem. Phys. **28**, 258 (1958).
[11] Y. Oono and S. Puri, Phys. Rev. Lett. **58**, 836 (1987).
[12] P. G. de Gennes, J. Chem. Phys. **72**, 4756 (1980).
[13] N. M. Maurits and J. G. E. M. Fraaije, J. Chem. Phys. **106**, 6730 (1997).
[14] J. G. E. M. Fraaije, J. Chem. Phys. **99**, 9202 (1993).
[15] J. G. E. M. Fraaije, B. A. C. van Vlimmeren, N. M. Maurits, M. Postma, O. A. Evers, C. Hoffmann, P. Altevogt, and G. Goldbeck-Wood, J. Chem. Phys. **106**, 4260 (1997).
[16] N. M. Maurits, B. A. C. van Vlimmeren, and J. G. E. M. Fraaije, Phys. Rev. E **56**, 816 (1997).
[17] N. M. Maurits and J. G. E. M. Fraaije, J. Chem. Phys. **107**, 5879 (1997).
[18] B. A. C. van Vlimmeren and J. G. E. M. Fraaije, Comput. Phys. Commun. **99**, 21 (1996).
[19] N. M. Maurits, P. Altevogt, O. A. Evers, and J. G. E. M. Fraaije, Comput. Theor. Polym. Sci. **6**, 1 (1996).
[20] T. Kawakatsu, Phys. Rev. E **56**, 3240 (1997).
[21] B. K. Annis, D. W. Schwark, J. R. Reffner, E. L. Thomas, and B. Wunderlich, Makromol. Chem. **193**, 2589 (1992).
[22] M. D. Foster, M. Sikka, N. Singh, F. S. Bates, S. K. Satija, and C. F. Majkrzak, J. Chem. Phys. **96**, 8605 (1992).
[23] T. L. Morkved, M. Lu, A. M. Urbas, E. E. Ehrichs, H. M. Jaeger, P. Mansky, and T. P. Russell, Science **273**, 931 (1996).
[24] A. Karim, N. Singh, M. Sikka, F. S. Bates, W. D. Dozier, and G. P. Felcher, J. Chem. Phys. **100**, 1620 (1994).
[25] A. M. Mayes, T. P. Russell, P. Bassereau, S. M. Baker, and G. S. Smith, Macromolecules **27**, 749 (1994).
[26] P. Mansky, P. Chaikin, and E. L. Thomas, J. Mater. Sci. **30**, 1987 (1995).
[27] T. Hashimoto, M. Fujimura, and H. Kawai, Macromolecules **13**, 1660 (1980).
[28] G. J. Kellogg, D. G. Walton, A. M. Mayes, P. Lambooy, T. P. Russell, P. D. Gallagher, and S. K. Satija, Phys. Rev. Lett. **76**, 2503 (1996).
[29] M. S. Turner, Phys. Rev. Lett. **69**, 1788 (1992).
[30] N. Koneripalli, N. Singh, R. Levicky, F. S. Bates, P. D. Gallagher, and S. K. Satija, Macromolecules **28**, 2897 (1995).
[31] H. Chen and A. Chakrabarti, Phys. Rev. E **55**, 5680 (1997).
[32] D. Petera and M. Muthukumar, J. Chem. Phys. **107**, 9640 (1997).
[33] G. Brown and A. Chakrabarti, Phys. Rev. A **46**, 4829 (1992).
[34] T. P. Russell, Curr. Opin. Colloid Interface Sci. **1**, 107 (1996).
[35] G. Brown, A. Chakrabarti, and J. F. Marko, Phys. Rev. E **50**, 1674 (1994).
[36] S. Puri and K. Binder, Phys. Rev. A **46**, R4487 (1992).
[37] Z. Jiang and C. Ebner, Phys. Rev. B **39**, 2501 (1989).
[38] P. Wiltzius and A. Cumming, Phys. Rev. Lett. **66**, 3000 (1991).
[39] C. Biver, R. Hariharan, J. Mays, and W. B. Russell, Macromolecules **30**, 1787 (1997).
[40] B. Q. Shi, C. Harrison, and A. Cumming, Phys. Rev. Lett. **70**, 206 (1993).
[41] S. M. Troian, Phys. Rev. Lett. **71**, 1399 (1993).
[42] R. Hasegawa and M. Doi, Macromolecules **30**, 3086 (1997).
[43] H. Kodama and S. Komura, J. Phys. II France **7**, 7 (1997).